Anal. Bioanal. Electrochem., Vol. 6, No. 6, 2014, 745-762

Analytical & Bioanalytical Electrochemistry

Full Paper

Numerical Modeling on Anodic Chronopotentiometric Transients for the Electrochemical Sensing of Methyl Salicylate

M. Kanagasabapathy[1,*], Y. Umasankar[2] and G. N. K. Ramesh Bapu[3]

[1]*Department of Chemistry, Rajus' College, Madurai Kamaraj University, Rajapalayam (TN) PIN 626 117, India*

[2] *Postdoctoral Research Associate, Nano Electrochemistry Laboratory, College of Engineering, University of Georgia, Athens, GA 30602, USA*

[3] *Senior Principal Scientist & Deputy Director, EMFT Division, Central Electrochemical Research Institute, Karaikudi (TN) PIN 630 006, India*

* Corresponding Author, Tel.:+ 91-94438 62183

E-Mails: rrcmks@gmail.com

Received: 16 August 2014/ Received in Revised form: 29 October 2014 / Accepted: 7 November 2014/ Published online: 31 December 2014

Abstract- A novel electrochemical sensing methodology for the detection of methyl salicylate concentration, [*MeS*] through chronopotentiometric transients under galvanostatic mode is devised. The oxidation potential shifted cathodically, with the increase in [*MeS*] due to the reduction in absolute anodic current density. Either if anodic current density (i_a) is lowered or [*MeS*] is enhanced, then the rate of oxidation is prevailed by diffusion control rather than charge-transfer limitations. The determined exchange current density was 7.9×10^{-4} A dm^{-2}. Discrete anodic oxidation current was estimated and is about 8.49 mA in the potential range 493 to 606 mV. I order chronopotentiometric transients are having comparatively larger (0.005 Volt $min.^{-1}$) and positive than the subsequent higher order transients at [*MeS*] = 7 mM and at i_a = 0.063 Adm^{-2}. The lower detection limit of 7 mM can be achieved with an absolute error 0.005. Off mode potential decay depends on [*MeS*] and i_a. The anodic oxidation of salicylate di-ion occurs through three electrons transfer whereas methoxide ion takes place through one electron transfer. Diclofenac shifts the anodic potential more negatively, even at low concentrations. Non-linear numerical simulations, to interpose anodic potential with [*MeS*] were carried out using MATLAB®.

Keywords- Methyl Salicylate, Electrochemical Sensor, Chronopotentiometry, Nnumerical Analysis

1. INTRODUCTION

Methyl salicylate is a prostaglandin biosynthesis inhibitor, used as effective analgesic / anti-inflammatory medication to treat muscular pains, athletic injuries [1] along with diclofenac. But *MeS* is highly toxic and its lethal dosage (LD_{50}) is about 101 mg/kg for adult human beings [2]. Most of the muscular pain reliving sprays or liniments formulation contains about 5–10 weight percent of *MeS* [3]. Monitoring of Methyl Salicylate, [*MeS*] concentration in the body is essential during acute poisoning [4] due to its excessive usage through medications. There were many reports of methyl salicylate poisoning [5] through anti–inflammatory medications. Detection methods of *MeS* based on HPLC, colorimetry, potentiostatic techniques were reported [6] and the electrochemical sensing is more dependable and prevalent [7]. Though many research works were mainly focused on acetyl salicylic acid determination based on potentiostatic approach, very few research reports were available on the electrochemical sensing of *MeS*. Veronika Supalkova, et al., had reported the detection of salicylic acid and *MeS* in the willow barks through potentiostatic analysis [7,8]. Recently, we had reported the electrochemical sensing of [*MeS*] at 7mM detection limit in plant volatiles using electroactive gold nano particles [9] under potentiostatic mode. But to the best of our knowledge, no studies based on galvanostatic mode was reported which is more cost effective, since constant current devices are more easily available and cheaper than potentiostats for real time analysis [10]. In this context, this work addresses a novel and reliable electrochemical sensing methodology for [*MeS*] based on galvanostatic mode, using low-cost graphite pencil anode rather than gold anodes to accomplish a better detection limit. Similarly, numerical analysis through MATLAB® are also designed to interpose the [*MeS*] and to enhance the accuracy as well as precision of the interpolation from the available anodic potential transients, since no works were reported based on non–linear numerical interpolations for electrochemical sensors.

2. EXPERIMENTAL

2.1. Materials

All the reagents used for this study are Analytical Grade and used as received without further purification. Methyl salicylate (Sigma Aldrich make) solution, with required concentration was prepared by dissolving the appropriate quantity in 0.1 M KOH (99 % Merck). To enhance the hydrolysis rate followed by anodic oxidation of methyl salicylate, 0.1 M KOH is chosen as it also enhances the specific conductivity and retards the ohmic

polarization potential. Sodium salt of diclofenac, (Merck Millipore make) was used to note the influence over anodic potential of methyl salicylate.

2.2. Instruments

Three electrodes cell assembly was used for the anodic oxidation. Graphite pencil electrode (GPA), (Make: Deep Vision Electrodes, India) of cylindrical shape with lateral surface area 1.65 cm^2 (radius–0.15 cm; height–1.75 cm) was used as anode. Platinum electrode (Systronics, India) of having same dimension to that of anode was used as counter electrode. Both electrodes were washed with acetone, wiped with soft filter paper and rinsed thoroughly with double distilled water prior to use. A saturated calomel electrode (SCE) was used as reference electrode. All the three electrodes were inserted and fixed firmly on a circular Teflon cap in such a way that the anode to cathode inter-electrode distance, 4.5 cm to nullify the ohmic polarization potential. And SCE was fixed proximately to that of anode at a distance of 1.5 cm, to minimize the IR drops. Then this cap along with the three electrodes was screwed tightly over a cylindrical electrochemical cell of capacity about 100 ml, made up of borosilicate glass. Constant current is maintained by using computer controlled single channel galvanostat, (Model: 2200-30-5, KEITHLEY Make, USA) and the anodic potential, (η_a) vs. SCE was recorded by using computer interfaced voltage logger (Model: DMM 2100, KEITHLEY Make, USA) for every one second time interval, up to 10 minutes time duration (t_d). Following the off mode, anodic potential decay (η_d) was recorded for every 1 second interval, up to 1 minute time duration. The value of [*MeS*] was optimized, for a significant shift in η_a values with reference to applied anodic current density (i_a) variations, ranging from 0.0315 A dm^{-2} (0.5 mA) to 0.2205 A dm^{-2} (3.5 mA). Before each run, a blank anodic potential using 0.1 M KOH alone was recorded at the given current density. Influence of diclofenac concentration [*Dic*] over transients was also recorded.

2.3. Software

Numerical correlations and interpolation of 'η_a' with transients and 'i_a' were analyzed through indigenously designed computer programs coded in MATLAB® uplinked with Microsoft® Excel. The following freeware programs were designed [11] for numerical simulations:

i. POLYNOM – n^{th} order polynomial
ii. CHIP – Cubic Hermite polynomial
iii. $SPLINE^3$ – Cubic spline interpolation
iv. LAGRANGE – Lagrange interpolation

3. RESULT AND DISCUSSION

3.1. Effect of [*MeS*] on η_a

It can be elucidated that η_a was shifted cathodically (Fig. 1) if [*MeS*] increased. This is due to the decrease in absolute anodic surface area, as anodic interface is enriched with $C_7H_4O_3^{2-}$ and CH_3O^- due to electromigration followed by adsorption over the surface at relatively higher [*MeS*] for the given i_a. But if i_a increased, then η_a was shifted anodically. The observed η_a values are 0.493 V and 0.576 V at the given i_a values of 0.063 Adm^{-2} and 0.126 Adm^{-2} respectively at [*Mes*] = 7 mM and t_d = 5 min. And the η_a value is lowered to 0.435 V at [*MeS*] = 14 mM and i_a = 0.063 Adm^{-2} at t_d = 5 min.

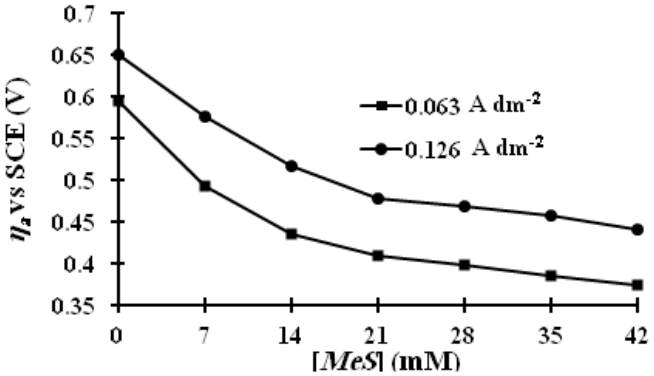

Fig. 1. η_a for [MeS] variations at t_d = 5 min

This in turn marginally decreases the absolute anodic current density (i_{ab}) used for oxidation from that of applied anodic current density, i_a. It should be emphasized that the trend in cathodic shift with [*MeS*] is unaffected by the variations in i_a. And the calculated first order derivatives, ($d\eta_a/d$[*MeS*]) were maximum and distinct (Fig. 2), at lower limits of d[*MeS*] even if i_a was relatively lower. But it became nearly constant, when [*MeS*] was above 28 mM. With the decrease in [*MeS*], value of i_{ab} drops which leads to enhance $d\eta_a$. This indicates, the absolute difference between i_a and i_{ab} is relatively lower, if [*MeS*] is low, due to low anodic surface coverage by the adsorbed ionic intermediates.

First order derivative values are significantly higher than the subsequent higher order derivatives for the given i_a. The value of $d\eta_a/d$[*MeS*] is 0.01443, when d[*MeS*] is about 7 mM but it is lowered to 0.01136 for d[*MeS*] is about 14 mM. It is further lowered to 0.0088 when d[*MeS*] is about 21 mM at a constant i_a of 0.063 A dm^{-2}. It should be emphasized that, if d[*MeS*] ≤ 5 mM, then the net η_a for both $C_7H_4O_3^{2-}$ and CH_3O^- is shifted towards OH^- anodic potential. At 3 mM the observed η_a iss about 561 mV with reference to 594 mV for 0.1 M OH^-. Hence the optimized lower detection limit for [*MeS*] is 7 mM at an i_a of 0.063 A dm^{-2}.

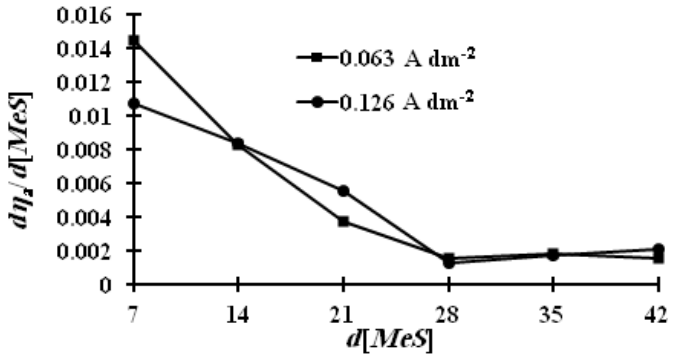

Fig. 2. First order derivatives of $d\eta_a/d[MeS]$

3.2. Effect of i_a on η_a

From the linearized Tafel plots (Fig. 3) it can be observed that if i_a increased, then η_a was shifted more anodically. The estimated exchange current density (i_o), from the Tafel plot is about 7.9×10^{-4} A dm^{-2}. This moderate exchange current density indicates that, the anodic oxidation rate is prevailed mainly by diffusion control rather than charge transport phenomena at lower [*MeS*] values. Overall anodic charge-transfer rate is relatively fast when compared to diffusion rate of $C_7H_4O_3^{2-}$ (di–ion) and CH_3O^- anions at relatively lower [*MeS*]. At higher [*MeS*], the electromigration rate is relatively retarded and enhances the mass-transport limitations associated with inter-ionic attractions, between the (K^+O^-) ($C_6H_4COO^-$ K^+) – ($CH_3O^-K^+$) species. But if [*MeS*] is lowered, then the η_a shifted anodically for the given i_a, by both dissociation rate as well as electromigration rate of ionic species and hence the anodic interface is enriched with $C_7H_4O_3^{2-}$ and CH_3O^- at the given i_a. So the oxidation rate depends on mainly charge–transfer processes rather than mass–transfer limitations.

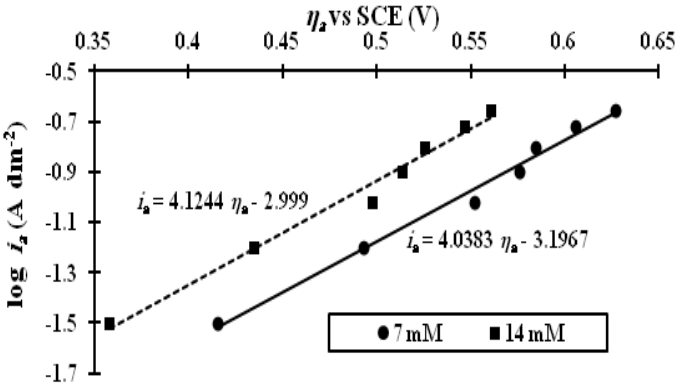

Fig. 3. Tafel plot for [*MeS*] variations at t_d = 5 min

Increase in η_a values with respect to i_a at a given [*MeS*] indicates that, the rate of oxidation is increased as electron transfer per mole is increased. This is because the difference between i_a *and* i_{ab} is reduced as more anodic surface is available for the oxidation with the increase in charge-transfer rate. I order to VI order derivatives for the variations in $d\eta_a$ with di_a (Fig. 4) were noted.

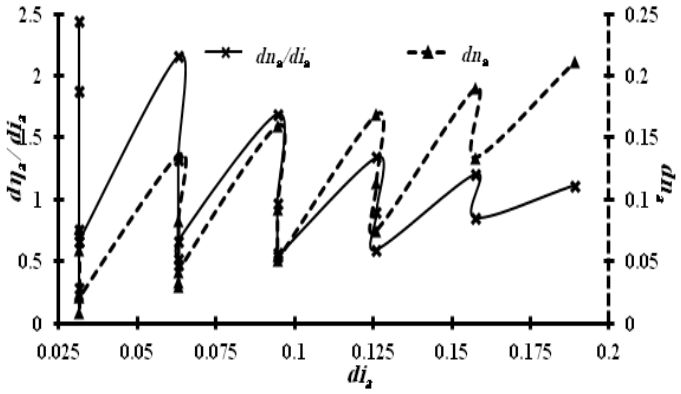

Fig. 4. $d\eta_a/di_a$ at [*MeS*] = 7 mM; t_d = 5 min

The value of ($d\eta_a$ /di_a) relatively higher with reference to I order di_a variations. The observed $d\eta_a$ is about 0.211 for VI order and it decreases to 0.077 for I order. But $d\eta_a/di_a$ is maximum at about 2.444 for I order and it drops to 1.116 for VI order. This facilitates the sensing of *MeS* at low concentration of about 7 mM with least deviation, using lower i_a.

3.3. Chronopotentiometric Transients

Oxidation potential increases slightly in the initial stages (126 – 142 seconds) and then drops very gradually (Fig. 5).

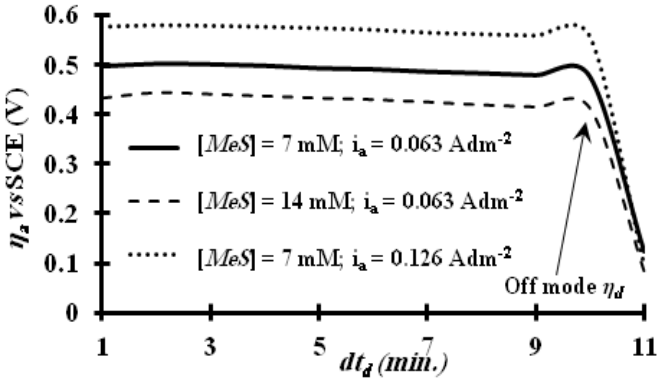

Fig. 5. Chronopotentiometric transients

This shows the overall process is under charge-transfer control in the initial stages of oxidation and then gradually turns into mixed charge and mass-transfer control as the reaction proceeds with time.

Chronopotentiometric transient curve for [*MeS*] at 7 mM always lies above 14 mM for the given i_a, 0.063 Adm^{-2}. This indicates at 14 mM, anodic interface is augmented with $C_7H_4O_3^{2-}$ as well as CH_3O^- species and the oxidation rate is governed by more diffusion flux when compared to [*MeS*] = 7mM, since anodic surface coverage and i_{ab} are relatively lower. And $d\eta_a/dt_d$ for I order to VIII order variance of dt_d at *[MeS]* = 7 mM and i_a = 0.063 Adm^{-2} exhibits (Fig. 6), a positive peak up to III order and after III order it doesn't exist. Moreover, I order variances are having comparatively large positive hump (0.005 Volt min.$^{-1}$) followed by II order variances (0.002 Volt min.$^{-1}$). At the same time, negative peaks are having relatively larger spread than their relevant positive peaks. Congruently, the negative shift for I order variance is maximum (0.005 Volt min.$^{-1}$), followed by II and III order variance values (0.004 Volt min.$^{-1}$). This shows the overall process is under charge-transfer control in the initial stages of oxidation and then gradually turns into mixed charge and mass-transfer control as the reaction proceeds with time. So, these I order dt_d variance can be more expedient to analyze [*MeS*] at comparatively low concentration under lower i_a values. From off-mode anodic potential decay rate, it can be implied that either at lower i_a or at lower [*MeS*], the value of η_d is moderately higher due to higher diffusion rate as well as charge–transfer rate. At [*MeS*] = 7 mM and at i_a = 0.063 Adm^{-2}, the η_d is about 0.124 V min.$^{-1}$ and it drops to 0.078 V min.$^{-1}$ at [*MeS*] = 14 mM and 0.097 V min.$^{-1}$ at i_a = 0.126 Adm^{-2}.

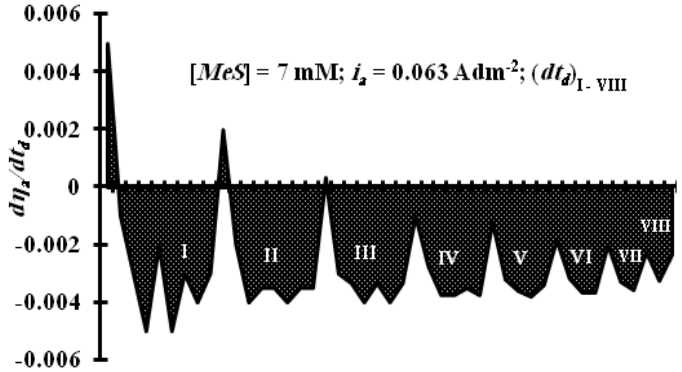

Fig. 6. $d\eta_a/dt_d$ for nth order dt_d variance

This can be characterized from Nernstian model for equilibrium potential under off-mode, based on the activities of oxidized species, $[MeS]_o$.

$\eta_d = \eta_d° + k_N \log_e [MeS] / [MeS]_o$ where, k_N is constant and equals to 6.5263×10^{-3} J. F^{-1}. mol^{-1} at 303 K for four electrons transfer (Refer Section 3.4). The decay potential under standard conditions, $\eta_d°$ (273 K and 1 M) is constant and i_{ab} as well as $[MeS]_o$ can be increased, if the value of i_a is raised. So it can be concluded that, the factors augmenting $[MeS]_o$ such as i_a, i_{ab}, η_a, t_d can lead to subside the η_d values.

3.4. Stoichiometric Analysis of Faradaic Electron Transfer Processes

From our recent studies, it can be noted [9] that the anodic oxidation of methyl salicylate leads to 1,4 benzoquionone derivative and formaldehyde. From this, the stoichiometry for mass transfer and electron transfer mechanistic steps, are given in Fig. 7.

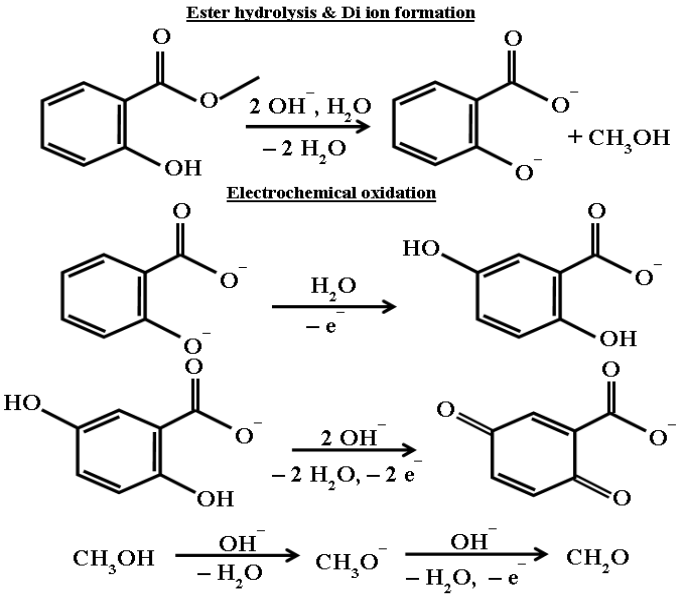

Fig. 7. Scheme for anodic oxidation of MeS

The salicylate di-ion after hydrolyzing, can loses an electron and initiated the formation of 1,4 benzhydroquinone derivative. Then in presence of OH^- ions 1,4 benzhydroquinone derivative as well as methoxide ion loses electrons to form 1,4 benzoquionone derivative and formaldehyde. Conversion of salicylate di-ion to benzhydroquinone encompasses three electrons transfer and methoxide oxidation involves one electron transfer. From the proposed scheme it can be elucidated that the di-ion oxidation rate mainly depends on charge-transfer processes, but the methoxide electron transfer is predominantly controlled by diffusion controlled migration of ions. This is because the charge–transfer kinetics of di-ion involves three electron–transfer followed by molecular rearrangement from hydroquinone to quinone transition. This elevates the activation polarization associated with electron transfer and molecular rearrangement. Due

to the single electron transfer, methoxide species get transformed into formaldehyde with relatively faster kinetics and charge-transfer rate. Hence, the interface is depleted with methoxide ion, if the charge-transfer rate proceeds over the diffusion rate but is enriched with di-ion intermediates with time.

So the overall concentration polarization is enhanced for CH_3O^- at higher charge transfer rate. This leads to retard the diffusion flux of methoxide species but favors for the electron transfer rate of di-ion, which are enriched in the vicinity of anode interface. So both charge and mass transfer rates are enhanced by the competitive adsorption of both anionic species from the interface vicinity towards anodic surface. Diffusion rate of di-ion is enhanced due to its higher charge and diffusion rate, but it has lower electron transfer rate. Stoichiometric electron-transfer can be estimated by, $[M_m \times C_e] / [n_e \times N_A]$

M_m – Molar mass of anionic species; N_A – Avogadro number

C_e – Number of electrons associated with one Coulomb – 6.2415×10^{18}

n_e – Number of electrons transferred per molecule

So about 4.70×10^{-4} moles of salicylate di-ion can be oxidized to benzhydroquinone derivative and 3.21×10^{-4} moles of methoxide can be oxidized to formaldehyde per Coulomb of charge-transfer. It can be elucidated that about 3.94×10^{-4} moles of MeS can be oxidized per Coulomb. Hence charge-transfer rate of CH_3O^- is nearly1.5 times faster than di-ion. The net anodic current associated with the oxidation of $[MeS] = 7$ mM at t_d =10 min. is about 29.61 mA.

3.5. Numerical Analysis on η_a and [*MeS*]

Numerical interpolation is prerequisite to predict the [*MeS*] with least deviation from the measured η_a and t_d during the real time sample analysis. Observed η_a data points are non-linear and have irregularly spaced values with reference to i_a or [*MeS*] or t_d. So, interpolating models of irregularly spaced variants were chosen for this simulation. It can be explicated [12-14] that Lagrange (L), quadratic / cubic spline (S^3), Cubic Hermite interpolation polynomial (*CHIP*), nth order polynomial (P^4 & P^5) models were more precise with higher accuracy than other non-linear interpolating models.

Though polynomial of higher nth order (or if n > 5) can be designed to improve both precision and accuracy, it suffers from Runge's error [14]. For interpolation analysis, (n–1) set of [*MeS*] for the given η_a or i_a or t_d data points were selected (from the 'n' set available), by excluding the chosen set of data points such as $[MeS]_x$ for $(\eta_a)_x$ or $(i_a)_x$ or $(t_d)_x$ which were used for interpolation analysis. All the available data points were analyzed to predict the deviation and from this, the error in the model can be analyzed.

Algorithms for Lagrangian, quadratic / cubic splines and nth order polynomial models were given in Appendixes 1 – 3. Iteration coefficients for $[MeS]_n$ interpolations using

these models can be computed through indigenously designed computer programs coded in MATLAB® [12–14]. Tables 1 and 2 show, interpolation analysis using models from the available experimental data points. And *[MeS]* data points as well as applied anodic current (I_a) were correlated to η_a (Tables 1 and 2).

Degree of deviation in the models for the given data point can be measured through absolute error (ε_{ab}) and absolute error average (ε_{av}) from the available data points (n_i).

$\varepsilon_{ab} = |\text{Actual value} - \text{Interpolated value}|$.

$\varepsilon_{av} = \{[\varepsilon_{ab}]_1 + [\varepsilon_{ab}]_2 \ldots [\varepsilon_{ab}]_{(n-2)} + [\varepsilon_{ab}]_{(n-1)} + [\varepsilon_{ab}]_{(n)}\} / n_i$

The value of ε_{ab} is higher at boundary conditions in all the models, but reduced in intermediate selections. In the interposing of η_a with $[MeS]_n$, *L* and P^5 and S^3 models shows best fit with comparatively lower ε_{av} of 0.005 and on the contrary *CHIP* model shows best fit with lower ε_{av} (0.005) for I_a data points correlation. It should be emphasized that, these models are more precise to predict the intermediate [*MeS*] data points, since the relative error is very low under these conditions.

Table 1. Interpolation analysis of η_a and $[MeS]_n$ at t_d = 5 min and i_a = 0.063 Adm^{-2}

#	[*MeS*] mM	η_a (V)	Predicted $[\eta_a]_x$ from models							
			L, P^5	ε_{ab}	P^4	$^*\varepsilon_{ab}$	CHIP	ε_{ab}	S^3	ε_{ab}
1.	0	0.594	0.579	0.015	0.617	0.023	0.571	0.023	0.599	0.005
2.	7	0.493	0.495	0.002	0.488	0.005	0.495	0.002	0.492	0.001
3.	14	0.435	0.434	0.001	0.438	0.003	0.439	0.004	0.436	0.001
4.	21	0.409	0.410	0.001	0.410	0.001	0.413	0.004	0.409	0.000
5.	28	0.398	0.397	0.001	0.395	0.003	0.396	0.002	0.395	0.003
6.	35	0.385	0.387	0.002	0.391	0.006	0.386	0.001	0.390	0.005
7.	42	0.374	0.359	0.015	0.348	0.026	0.370	0.004	0.353	0.021
			$^{**}\varepsilon_{av}$ = 0.005		**ε_{av} = 0.010**		**ε_{av} = 0.006**		**ε_{av} = 0.005**	

$^*\varepsilon_{ab}$ = Absolute error in the models; $^{**}\varepsilon_{av}$= Absolute error average in the models
L – Lagrangian; P^5 & P^4 – 5th & 4th order;
S^3 – Cubic spline polynomial; CHIP – Cubic Hermite

Table 2. Interpolation analysis of η_a and $(I_a)_n$ at t_d = 5 min. and [*MeS*] = 7 mM

#	I_a mA	η_a (V)	Predicted $[\eta_a]_x$ from models							
			L, P^5	ε_{ab}	P^4	ε_{ab}	CHIP	ε_{ab}	S^3	ε_{ab}
1.	0.5	0.416	0.432	0.016	0.348	0.068	0.414	0.002	0.384	0.032
2.	1.0	0.493	0.490	0.003	0.508	0.015	0.499	0.006	0.500	0.007
3.	1.5	0.552	0.553	0.001	0.544	0.008	0.545	0.007	0.547	0.005
4.	2.0	0.576	0.575	0.001	0.575	0.001	0.571	0.005	0.575	0.001
5.	2.5	0.585	0.586	0.001	0.594	0.009	0.591	0.006	0.590	0.005
6.	3.0	0.606	0.603	0.003	0.590	0.016	0.602	0.004	0.597	0.009
7.	3.5	0.627	0.643	0.016	0.698	0.071	0.634	0.007	0.665	0.038
			ε_{av} = 0.006		**ε_{av} = 0.027**		**ε_{av} = 0.005**		**ε_{av} = 0.014**	

3.6. Determination of Discrete Anodic Current (I_a)

Discrete anodic current values (I_a) can be computed to estimate the oxidation rate of *[MeS]* at the given η_a as well as t_d. From this the Coulombs required for the oxidation can be determined at the given potential irrespective of other factors. The available η_a values can be analyzed using the maximum available data points (j_m) through the quadratic polynomial (Appendix 3: for 2nd degree) with respect to I_a:

$$I_a = \int_{x_i}^{x_j} .[a\ \eta_a^2 + b\ \eta_a + c]\ d\eta_a \rightarrow (1)$$

The equation (1) under these boundary conditions leads to,

$$= \left[(a\ \eta_a^3/3) + (b\ \eta_a^2/2) + (c\ \eta_a)\right]_{x_i}^{x_j} \rightarrow (2)$$

The solution for equation (2) is valid for any intervals of η_a between x_i and x_j of where $i \neq 0$; $i \neq j$; $i < j$ *and* $j < j_m$. The estimated values of a, b and c are 77.596, 66.857and 14.929 respectively within the potential range taken. The net anodic current associated with the oxidation is about 8.49 mA in the potential range 493 to 606 mV.

3.7. Effect of Diclofenac on η_a

Most of the muscular pain reliving formulation contains *MeS* along with diclofenac [3] with the [*Dic*] to [*MeS*] ratio, 1:10. Hence, it is necessary to determine the influence of [*Dic*] over η_a. So η_a was recorded with [*Dic*] variations, 0.7 and 1.4 mM at i_a = 0.063 and 0.126 Adm^{-2} with [*MeS*] at 7 mM. Anodic potential significantly shifted more negatively by the presence of diclofenac. About 150 mV anodic shift in net η_a was observed, by the presence of [*Dic*] at 0.7 mM even at lower current density, i_a = 0.063 Adm^{-2}. If [*Dic*] was increased, then η_a further shifted towards negative direction and this is depicted in Fig. 8.

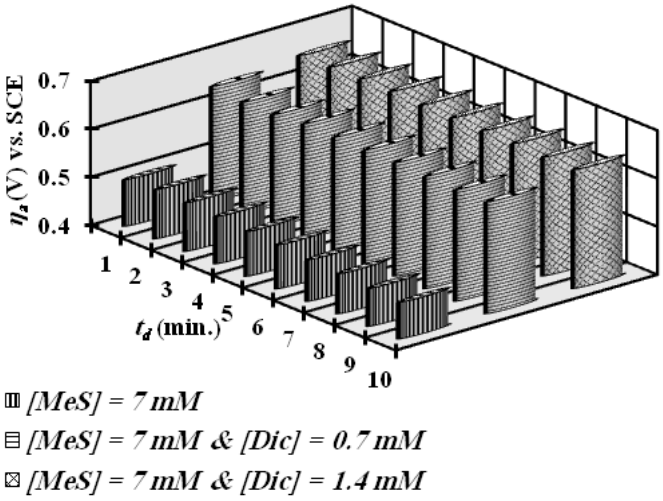

Fig. 8. Effect of [*Dic*] on η_a at i_a = 0.063 Adm^{-2}

Effect of i_a on η_a as well as η_d at [*Dic*] = 0.7 mM was given in Fig 9. With the increase of i_a from 0.063 Adm^{-2} to 0.126 Adm^{-2}, η_a was moved towards more anodically to about – 210 mV at t_d = 10 min. Similarly, potential decay, η_d was also increased from 0.176 V to 0.197 V with the increase in i_a from 0.063 Adm^{-2} to 0.126 Adm^{-2} when compared to 0.124 V in the absence of diclofenac at i_a = 0.063 Adm^{-2}. This aids the sensing of [*MeS*] distinctly with a shift in anodic potential to about – 200 mV, even at low [*Dic*] value of 0.7 mM. And this indicates diclofenac actively influences the anodic oxidation potential of methyl salicylate even at very low concentration. Further studies are now on the way, to analyze the oxidation patterns of MeS in the presence of diclofenac using spectral data.

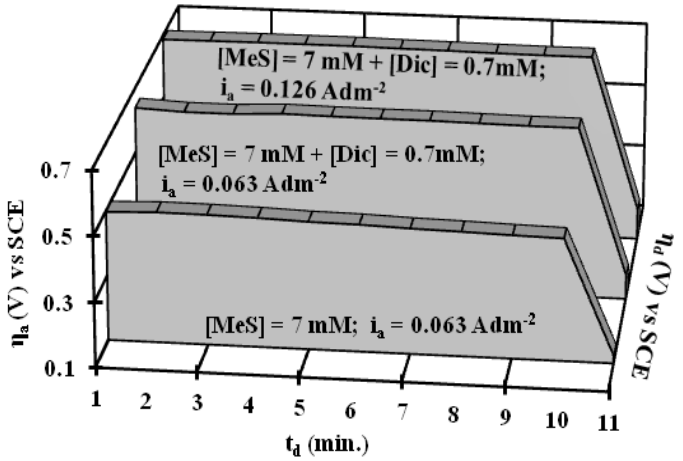

Fig. 9. Effect of i_a on η_a and η_d at [*Dic*] = 0.7 mM

4. CONCLUSION

A novel and cost-effective electrochemical sensing methodology for the detection of methyl salicylate concentrations, [*MeS*] in pharmaceutical formulations, through anodic oxidative chronopotentiometric transients under galvanostatic mode using graphite pencil anode is devised. Average exchange current density is determined and is about 7.9×10^{-4} A dm^{-2}. Either if anodic current density is lowered or [*MeS*] is enhanced, then the rate of oxidation is prevailed by diffusion control rather than charge-transfer limitations. Anodic potential (η_a) is shifted towards cathodically with reference to [*MeS*]. Value of $d\eta_a$ is large for higher order variance and is about 0.211 volt for VI order but decreases to 0.077 volt for I order variance. The lower detection limit of 7 mM can be achieved with a negligible absolute error of 0.005. The anodic potential variance ($d\eta_a$) is also distinct for this lower detection limit value at 7 mM. The transients variance for I order is relatively large with a significant positive hump at 0.005 Volt min.$^{-1}$ when compared to higher order variations. Off mode potential decay depends on both apparent current density as well as [*MeS*]. From electron-transfer stoichiometry, about 4.70×10^{-4} moles/C of salicylate di-ion can be

oxidized to benzhydroquinone derivative through three electrons transfer and 3.21×10^{-4} moles/C of methoxide can be oxidized to formaldehyde by one electron transfer. Di–ion oxidation is significantly influenced by activation polarization due to slow electron transfer followed by benzoquionone formation. Oxidation potential was shifted anodically to about 200 mV in the presence of diclofenac even at lower (0.7 mM) concentration. Non-linear best fit models, Lagrange, n^{th} order polynomial, quadratic/cubic splines and cubic Hermite interpolation polynomial were designed, by using MATLAB® to correlate anodic potential with anodic current and [*MeS*]. Deviations in the models are very low with an absolute error of about 0.005. Discrete anodic current for the oxidation is estimated and is about 8.45 mA between the potential range 493 to 606 mV.

REFERENCES

[1] L. Mason, R. A. Moore, J. E. Edwards, H. J. McQuay, S. Derry, and P. J. Wiffen, Brit. Med. J. 328 (2004) 995.

[2] Material Safety Data Sheet: Product Number: 76631; CAS-No.: 119-36-8, Sigma–Aldrich, [online] available: www.sigma-aldrich.com.

[3] Salonpas® Pain Relief Patch, Hisamitsu Pharmaceutical Co., Inc., [online] available:http://www.hisamitsu.co.jp/english/products/salonpas_pain_relief_patch.html

[4] R. F. Carvalhal, A. L. de Jesus de Almeida, and N. H. Moreira, Biosens. Bioelect. 25 (2010) 2200.

[5] D. Parker, C. Martinez, C. Stanley, J. Simmon, and L. M. Mclntyre, J. Anal. Toxicol. 28 (2004) 214.

[6] S. Kattuvilakam Abbas, and S. Sundaram Rengitham, J. App. Pharm. Sci. 4 (2014) 52.

[7] V. Supalkova, J. Petrek, L. Havel, S. Krizkova, J. Petrlova, and V. Adam, Sensors 6 (2006) 1483.

[8] J. Petrek, L. Havel, J. Petrlova, V. Adam, D. Potesil, P. Babula, and R. Kizek, Russ. J. Plant Physiol. 54 (2007) 553.

[9] Y. Umasankar, and R. P. Ramasamy, Analyst 138 (2013) 6199.

[10] D. Pletcher, Southampton Electrochemistry Group, Instrumental methods in Electrochemistry, Woodhead Publishing, Cambridge (2011).

[11] M. Kanagasabapathy, Technical computations by MATLAB, Math Forum (Research), Drexel University, Philadelphia, USA, [online] available: http://mathforum.org/library/view/75575.html, (2012).

[12] S. C. Chapra, and R. P. Canale, Numerical methods for Engineers, McGraw-Hill, New York (2006).

[13] M. Kanagasabapathy, G. N. K. Ramesh Bapu, P. Linga, and R. M. Gnanamuthu, Port. Electrochim. Acta, 30 (2012) 295.

[14] M. Kanagasabapathy, G. N. K. Ramesh Bapu, R. Sivan and, K. Sivaramamoorthy, Surf. Coat. Technol. 232 **(**2013**)** 188-197.

Appendixes

Appendix 1: Lagrangian algorithm

η_a data points are discrete, independent and unevenly spaced, for the given *[MeS]*. For 'n' number of data points, $(\eta_a)_1$, $(\eta_a)_2$, … $(\eta_a)_{(n-1)}$, $(\eta_a)_n$ the respective indeterminate $[MeS]_1$, $[MeS]_2$, … $[MeS]_{(n-1)}$, $[MeS]_n$ values can be interposed by the following algorithm.

Algorithm for Lagrangian model

$$[MeS]_x = f(\eta_a)_x = \frac{\{[(\eta_a)_x - (\eta_a)_2]\,[(\eta_a)_x - (\eta_a)_3]\ldots[(\eta_a)_x - (\eta_a)_{(n-1)}]\,[(\eta_a)_x - (\eta_a)_n]\}}{\{[(\eta_a)_1 - (\eta_a)_2]\,[(\eta_a)_1 - (\eta_a)_3]\ldots[(\eta_a)_1 - (\eta_a)_{(n-1)}]\,[(\eta_a)_1 - (\eta_a)_n]\}}[MeS]_1$$

$$+ \frac{\{[(\eta_a)_x - (\eta_a)_1]\,[(\eta_a)_x - (\eta_a)_3]\ldots[(\eta_a)_x - (\eta_a)_{(n-1)}]\,[(\eta_a)_x - (\eta_a)_n]\}}{\{[(\eta_a)_2 - (\eta_a)_1]\,[(\eta_a)_2 - (\eta_a)_3]\ldots[(\eta_a)_2 - (\eta_a)_{(n-1)}]\,[(\eta_a)_2 - (\eta_a)_n]\}}[MeS]_2 + \ldots$$

$$\ldots + \frac{\{[(\eta_a)_x - (\eta_a)_1]\,[(\eta_a)_x - (\eta_a)_2]\ldots[(\eta_a)_x - (\eta_a)_{(n-3)}]\,[(\eta_a)_x - (\eta_a)_{(n-2)}]\,[(\eta_a)_x - (\eta_a)_n]\}}{\{[(\eta_a)_{(n-1)} - (\eta_a)_1]\,[(\eta_a)_{(n-1)} - (\eta_a)_2]\ldots[(\eta_a)_{(n-1)} - (\eta_a)_{(n-2)}]\,[(\eta_a)_{(n-1)} - (\eta_a)_n]\}}[MeS]_{(n-1)}$$

$$(\eta_a) \quad + \frac{\{[(\eta_a)_x - (\eta_a)_1]\,[(\eta_a)_x - (\eta_a)_2]\ldots[(\eta_a)_x - (\eta_a)_{(n-3)}]\,[(\eta_a)_x - (\eta_a)_{(n-2)}]\,[(\eta_a)_x - (\eta_a)_{(n-1)}]\}}{\{[(\eta_a)_n - (\eta_a)_1]\,[(\eta_a)_n - (\eta_a)_2]\ldots[(\eta_a)_n - (\eta_a)_{(n-3)}]\,[(\eta_a)_n - (\eta_a)_{(n-2)}]\,[(\eta_a)_n - (\eta_a)_{(n-1)}]\}}[MeS]_n$$

for 'n' data points and $[MeS]_x$ as $f_n(\eta_a)_x$ is expressed in terms of 'x' as

$$f_n(\eta_a)_x = \sum_{i=0}^{n} L_i(x)\, f(x_i) \rightarrow 3$$

$$L_i(x) = \prod_{\substack{j=0 \\ j\neq 1}}^{n} [x - x_j] \,/\, [x_i - x_j] \rightarrow 4$$

In equation (4), $L_i(x)$ is Lagrange weighing function and this co-efficient includes a product of $(n-1)$ terms with terms of $j = i$ omitted.

Appendix 2: Quadratic / cubic splines algorithm

A quadratic polynomial approximates the data between two consecutive points, for a set of 'n' data, comprises $(\eta_a)_n$ and $[MeS]_n$ as:

$[(\eta_a)_1, [MeS]_1], [(\eta_a)_2, [MeS]_2], \ldots[(\eta_a)_{(n-1)}, [MeS]_{(n-1)}], [(\eta_a)_n, [MeS]_n]$.

For 'n' number of data points, (n–1) splines should pass and the sequential data points are correlated from quadratic equations solved by matrix formulation in the interpolation of $[MeS]_x$ from f $((\eta_a)_x)$ using the following quadratic spline algorithm.

Cubic splines can be originated as: $a_n[(\eta_a)_n]^3 + b_n[(\eta_a)_n]^2 + c_n(\eta_a)_n + d_n = [MeS]_n$

Algorithm for quadratic spline model

$(\eta_a)_1 \leq (\eta_a)_x \leq (\eta_a)_2 : a_1[(\eta_a)_1]^2 + b_1(\eta_a)_1 + c_1 = [MeS]_1$ & $a_1[(\eta_a)_2] + b_1(\eta_a)_2 + c_1 = [MeS]_2$

$(\eta_a)_2 \leq (\eta_a)_x \leq (\eta_a)_3 : a_2[(\eta_a)_2]^2 + b_2(\eta_a)_2 + c_2 = [MeS]_2$ & $a_2[(\eta_a)_3]^2 + b_2(\eta_a)_3 + c_2 = [MeS]_3$

……

$(\eta_a)_{(n-2)} \leq (\eta_a)_x \leq (\eta_a)_{(n-1)} : a_{(n-2)}[(\eta_a)_{(n-2)}] + b_{(n-2)}(\eta_a)_{(n-2)} + c_{(n-2)} = [MeS]_{(n-2)}$ & $a_{(n-2)}[(\eta_a)_{(n-1)}]^2 + b_{(n-2)}(\eta_a)_{(n-1)} + c_{(n-2)} = [MeS]_{(n-1)}$

$(\eta_a)_{(n-1)} \leq (\eta_a)_x \leq (\eta_a)_n : a_{(n-1)}[(\eta_a)_{(n-1)}]^2 + b_{(n-1)}(\eta_a)_{(n-1)} + c_{(n-1)} = [MeS]_{(n-1)}$ & $a_{(n-1)}[(\eta_a)_n]^2 + b_{(n-1)}(\eta_a)_n + c_{(n-1)} = [MeS]_n$

Continuous derivatives from interior data points:

$2a_1(\eta_a)_2 + b_1 - 2a_2(\eta_a)_2 - b_2 = 0$ at $(\eta_a)_2$

$2a_2(\eta_a)_3 + b_2 - 2a_3(\eta_a)_3 - b_3 = 0$ at $(\eta_a)_3$ ...

... $2a_{(n-2)}(\eta_a)_{(n-1)} + b_{(n-2)} - 2a_{(n-1)}(\eta_a)_{(n-1)} - b_{(n-1)} = 0$ at $(\eta_a)_{(n-1)}$

$2a_{(n-1)}(\eta_a)_n + b_{(n-1)} - 2a_n(\eta_a)_n - b_n = 0$ at $(\eta_a)_n$

First spline, $a_1[(\eta_a)_1]^2 + b_1(\eta_a)_1 + c_1 = [MeS]_1$ is linear and $a_1 = 0$ and the matrix solution is:

$$
\begin{array}{cccccccccccc}
0 & (\eta_a)_1 & 1 & 0 & 0 & 0 & 0 & 0 & 0\ldots & 0 & 0 & 0 = [MeS]_1 \\
[(\eta_a)_2]^2 & (\eta_a)_2 & 1 & 0 & 0 & 0 & 0 & 0 & 0\ldots & 0 & 0 & 0 = [MeS]_2 \\
0 & 0 & 0 & [(\eta_a)_2]^2 & (\eta_a)_2 & 1 & 0 & 0 & 0\ldots & 0 & 0 & 0 = [MeS]_2 \\
0 & 0 & 0 & [(\eta_a)_3]^2 & (\eta_a)_3 & 1 & 0 & 0 & 0\ldots & 0 & 0 & 0 = [MeS]_3 \\
0 & 0 & 0 & 0 & 0 & 0 & [(\eta_a)_3]^2 & (\eta_a)_3 & 1\ldots & 0 & 0 & 0 = [MeS]_3 \\
0 & 0 & 0 & 0 & 0 & 0 & [(\eta_a)_4]^2 & (\eta_a)_4 & 1\ldots & 0 & 0 & 0 = [MeS]_4 \\
\ldots\ldots & & & & & & & & & & & \\
0 & 0 & 0 & 0 & 0 & 0 & 0 & 0 & 0\ldots & [(\eta_a)_{(n-1)}]^2 & (\eta_a)_{(n-1)} & 1 = [MeS]_{(n-1)} \\
0 & 0 & 0 & 0 & 0 & 0 & 0 & 0 & 0\ldots & [(\eta_a)_n]^2 & (\eta_a)_n & 1 = [MeS]_n \\
2(\eta_a)_2 & 1 & 0 & -2(\eta_a)_2 & -1 & 0 & 0 & 0 & 0\ldots & 0 & 0 & 0 = 0 \\
0 & 0 & 0 & 2(\eta_a)_3 & 1 & 0 & -2(\eta_a)_3 & -1 & 0\ldots & 0 & 0 & 0 = 0 \\
0 & 0 & 0 & 0 & 0 & 0 & 2(\eta_a)_4 & 1 & 0\ldots & 0 & 0 & 0 = 0 \\
\ldots\ldots & & & & & & & & & & & \\
0 & 0 & 0 & 0 & 0 & 0\ldots & 2(\eta_a)_{(n-1)} & 1 & 0 & -2(\eta_a)_{(n-1)} & -1 & 0 = 0
\end{array}
$$

Algorithm for cubic spline model

$$[MeS]_x = f\,(\eta_a)_x = \frac{1}{6h}\,[((\eta_a)_i - (\eta_a)_x)^3\,M_{(i-1)} + \left((\eta_a)_x - (\eta_a)_{(i-1)}\right)^3 M_i + ((\eta_a)_i - (\eta_a)_x)\left(6[MeS]_{(i-1)} - h^2 M_{(i-1)}\right) + \left((\eta_a)_x - (\eta_a)_{(i-1)}\right)(6[MeS]_i - h^2 M_i)]$$

$M_1 = 0 = M_4$ at $1 \le (\eta_a)_i \le 4$ or $M_1 = 0 = M_3$ at $1 \le (\eta_a)_i \le 3$ etc.,

where, $h^2\left[M_{(i+1)} + 4M_i + M_{(i-1)}\right] = 6\left[\,[MeS]_{(i+1)} - 2\,[MeS]_i + [MeS]_{(i-1)}\right]$

for two successive sub intervals: $1 \le (\eta_a)_i \le 2$ *and* $2 \le (\eta_a)_i \le 3$ *...*

And 'h' is the difference between the two successive $(\eta_a)_i$ *values.*

Appendix 3: nth order polynomial algorithm

Polynomial Legendre equations of nth order [where n = (number of 'η_a' data points –1)] were deduced to correlate the given $[MeS]_x$.

$\partial i = \{[MeS]_i - (k_1 [(\eta_a)_i]^2 + k_2 (\eta_a)_i + k_3)\}$ where 'i' refers 1, 2, 3…n data points and k_1, k_2, k_3 are the pertinent co-efficient values for second degree parabola fit. The quadratic equation derived for this condition as: $\sum \partial i^2 = \sum\{[MeS]_i - (k_1[(\eta_a)_i]^2 - k_2 (\eta_a)_i - k_3)\}^2 = R_e$ By the principle of least squares, the value of 'R_e' (regression) should be minimum.

$$\partial R_e/\partial k_1 = -2\sum \{[MeS]_i - (k_1[(\eta_a)_i]^2 - k_2 (\eta_a)_i - k_3)\ ([MeS]_i)^2 = 0 \rightarrow 5$$

$$k_1\sum [(\eta_a)_i]^4 + k_2\sum[(\eta_a)_i]^3 + k_3\sum[(\eta_a)_i]^2 = \sum \{[(\eta_a)_i]^2\ [MeS]_i\} \rightarrow 6$$

Under the conditions $\partial R_e/\partial k_2 = 0$ and $\partial R_e/\partial k_3 = 0$ yields,

$$k_1\sum [(\eta_a)_i]^3 + k_2\sum[(\eta_a)_i]^2 + k_3\sum(\eta_a)_i = \sum \{(\eta_a)_i\ [MeS]_i\}$$

$$k_1\sum [(\eta_a)_i]^2 + k_2\sum(\eta_a)_i + nk_3 = \sum [MeS]_1 \rightarrow 7$$

The nth order polynomial can be formulated to determine $[MeS]_x$ as a function of potential $(\eta_a)_x$ and the co-efficient obtained from 'i' number of '$(\eta_a)_i$, (where, $n = [i - 1]$) as:

$$[MeS]_x = k_{(n-1)}\ [(\eta_a)_x]^{(n-1)} + k_{(n-2)}\ [(\eta_a)_x]^{(n-2)} + \ldots + k_2\ [(\eta_a)_x]^2 + k_1\ (\eta_a)_x + k$$